Mixing layer transport flux of particulate matter in Beijing, China

Yusi Liu[1], Guiqian Tang[2,3], Libo Zhou[2], Bo Hu[2], Baoxian Liu[4,5], Yunting Li[4,5], Shu Liu[6], Yuesi Wang[2,3,7]

[1] State Key Laboratory of Severe Weather & Key Laboratory for Atmospheric Chemistry of China Meteorology Administration, Chinese Academy of Meteorological Sciences, Beijing 100081, China

[2] State Key Laboratory of Atmospheric Boundary Layer Physics and Atmospheric Chemistry, Institute of Atmospheric Physics, Chinese Academy of Sciences, Beijing 100029, China

[3] Center for Excellence in Urban Atmospheric Environment, Institute of Urban Environment, Chinese Academy of Sciences, Xiamen 361021, China

[4] Beijing Municipal Environmental Monitoring Centre, Beijing 100048, China

[5] Beijing Key Laboratory of Airborne Particulate Matter Monitoring Technology, Beijing 100048, China

[6] Liaoning Provincial Environmental Monitoring & Experiment Center, Shenyang 110031, China

[7] University of Chinese Academy of Sciences, Beijing 100049, China

Correspondence: Guiqian Tang (tgq@dq.cern.ac.cn)

18   **Abstract**

19   Quantifying the transport flux (TF) of atmospheric pollutants plays an important role in

20   understanding the causes of air pollution and in making decisions regarding the prevention and

21   control of regional air pollution. In this study, the mixing layer height and wind profile were

22   measured by a ceilometer and Doppler wind radar, respectively, and the characteristics of the

23   atmospheric dilution capability were analyzed using these two datasets. The ventilation coefficient

24   (VC) appears to be highest in the spring (3940 ± 2110 m^2 s^{-1}) and lower in the summer (2953 ± 1322

25   m^2 s^{-1}), autumn (2580 ± 1601 m^2 s^{-1}) and winter (2913 ± 3323 m^2 s^{-1}). Combined with the

26   backscatters measured by the ceilometer, vertical profiles of the $PM_{2.5}$ concentration were obtained

27   and the $PM_{2.5}$ TF in the mixing layer was calculated. The TF was the highest in the spring at $4.33 \pm$

28   0.69 mg $m^{-1}s^{-1}$ and lower in the summer, autumn and winter, when the TF values were 2.27 ± 0.42

29   mg $m^{-1}s^{-1}$, 2.39 ± 0.45 mg $m^{-1}s^{-1}$ and 2.89 ± 0.49 mg $m^{-1}s^{-1}$, respectively. Air pollutants transport

30   mainly occurs between 14:00 and 18:00 LT. The TF was large in the pollution transition period

31   (spring: 5.50 ± 4.83 mg $m^{-1}s^{-1}$, summer: 3.94 ± 2.36 mg $m^{-1}s^{-1}$, autumn: 3.72 ± 2.86 mg $m^{-1}s^{-1}$ and

32   winter: 4.45 ± 4.40 mg $m^{-1}s^{-1}$) and decreased during the heavy pollution period (spring: 4.69 ± 4.84

33   mg $m^{-1}s^{-1}$, summer: 3.39 ± 1.77 mg $m^{-1}s^{-1}$, autumn: 3.01 ± 2.40 mg $m^{-1}s^{-1}$ and winter: 3.25 ± 2.77

34   mg $m^{-1}s^{-1}$). Our results indicate that the influence of the air pollutants transport in the southern

35   regions should receive more focus in the transition period of pollution, while local emissions should

36   receive more focus in the heavy pollution period.

37   **1. Introduction**

38   With the rapid development of its economy and industry, as well as its unique local topography,

39   Beijing has become one of the cities in the world that is most seriously affected by air pollution. As

40   early as before the 2008 Olympic Games, to fulfill the promise of a "Green Olympics", Beijing's

41   industries were relocated to surrounding provinces and cities. After the Olympic Games, with the

42   promulgation of the "Action Plan for Prevention and Control of Air Pollution", Beijing

43   implemented a series of measures to reduce pollutants, such as raising the emission standards of

44   motor vehicles and fuel standards for vehicles, changing coal to natural gas, coal to electricity and

45   so on. These measures have gradually improved Beijing's air quality, with the annual average fine

46   particulate matter ($PM_{2.5}$) concentration decreasing from 90 μg m^{-3} in 2013 to 58 μg m^{-3} in 2017

47   (Cheng et al. 2018a).

48   Although the Beijing government has been committed in recent years to taking measures that could

49   ensure a steady improvement in the air quality, there is still great pressure to achieve a continuous

50   decline in the particulate matter concentration. Beijing is in the north of the North China Plain, with

51   the south side and the west side the Yanshan Mountains and the Taihang Mountains, respectively.

52   Affected by the mountains to the northwest, there are more subsiding airflows, a lower mixing layer

53   height and an extremely limited atmospheric dilution capability. In addition, pollutants tend to

54   accumulate in front of the mountains due to the influence of southerly winds and the mountain

55   obstructions. In central and northern China, the increase in $PM_{2.5}$ during the winter is closely related

56   to the adverse atmospheric dilution conditions (Wang et al. 2016). Therefore, in addition to the

57   primary emissions and secondary formation, the weak atmospheric dilution capability is also an

58   important factor leading to the frequent occurrence of serious air pollution in Beijing.

59   In recent decades, the mixing layer height (MLH) and wind speed (WS) have been two major factors

leading to the annual increases in the aerosol concentration and polluted days during the winter in China (Yang et al. 2016). The low MLH and low WS are also important characteristics of the weak atmospheric dilution capability (Huang et al. 2018; Liu et al. 2018; Song et al. 2014; Tang et al. 2015). The change in the MLH represents the vertical dilution capability of pollutants, and the change in the WS represents the horizontal dilution capability of pollutants. The ventilation coefficient (VC) is usually used to evaluate the vertical and horizontal dilution capability of the atmosphere (Nair et al. 2007; Tang et al. 2015; Zhu et al. 2018). Thus, it is a good choice to use the VC to evaluate the relationship between the atmospheric dilution capability and air pollution in Beijing. Although previous studies have analyzed the relationship between the MLH and pollutants (Geiß et al. 2017; Miao and Liu 2019; Schäfer et al. 2006; Su et al. 2018), studies on the effects of the VC on the particle concentration have been extremely rare.

Although the problem of heavy pollution in northern China has improved in recent years, regional pollution problems remain, especially in the Beijing-Tianjin-Hebei region (Shen et al. 2019). There are three main transport routes affecting Beijing: the northwest path, the southwest path and the southeast path (Chang et al. 2018; Li et al. 2018; Zhang et al. 2018). The occurrence of heavy pollution in Beijing is closely related to the transport of pollutants in the southern regions, mainly in southern Hebei, northern Henan and western Shandong, while the high-speed northwest air mass is conducive to the removal of pollutants from Beijing (Li et al. 2018; Ouyang et al. 2019; Zhang et al. 2018; Zhang et al. 2017). In recent years, the contribution of regional transport to Beijing has been increasing annually, with a trend of 1.2% per year, which reached 31-73% in the summer and 27-59% in the winter (Chang et al. 2018; Cheng et al. 2018b; Wang et al. 2015). High $PM_{2.5}$ concentrations are usually accompanied by high transport flux (TF) within a day in Beijing. As pollution worsens, the contribution of the surrounding areas to the $PM_{2.5}$ in Beijing has risen from 52% to 65% in a month on average in 2016 (Zhang et al. 2018). However, during heavy pollution, the TF decreases in Beijing (Chang et al. 2018; Tang et al. 2015; Zhu et al. 2016).

To solve the regional pollution problem, joint prevention and control have been recommended for a long time. Many studies on regional transport have been carried out, but most observational studies cannot easily quantify the TF due to the lack of particle and wind vertical profiles, and it is still unclear when we need to control the emission sources and in which areas. To solve the above problems, we conducted 2 years of continuous observations on MLH and wind profiles in the Beijing mixing layer and analyzed the mixing layer dilution capability of the atmosphere. Afterwards, using the backscattering coefficient profile, we obtained the vertical $PM_{2.5}$ concentration profiles and calculated the TF profile and mixing layer TF. Finally, using the near-surface $PM_{2.5}$ concentration as an indicator to classify the air pollution degree, we analyzed the TF during the transitional and heavily polluted periods in Beijing and illuminated the main controlling factors.

2. Methods

2.1 Observational station

To understand the dilution capability characteristics in Beijing, two years of observations were conducted (2016.1.1-2017.12.31). The observational site (BJT) is at the Institute of Atmospheric Physics of the Chinese Academy of Sciences, located west of the Jiande Bridge in the Haidian

District, Beijing (39.98° N, 116.38° W). The north and south sides of the station are the north Third and north Fourth Ring Roads, respectively, and the eastern side is the Beijing-Tibet Expressway. The altitude (a.s.l.) is approximately 60 m. There is no obvious emission source around the observational site except for motor vehicles.

2.2 Observations of MLH and wind profiles

To analyze the dilution capability, the MLH was observed by a single-lens ceilometer (CL51, Vaisala, Finland), and the wind profile was simultaneously observed by a Doppler wind radar (Windcube 100s, Leosphere, France).

A single-lens ceilometer measures the attenuated backscatter coefficient profile of the atmosphere by pulsed diode laser lidar technology (910 nm waveband) within a 7.7 km range and determines the MLH through the positions of abrupt changes in the backscattering coefficient profile. In the actual measurement, the measurement interval was 16 s, and the measurement resolution was 10 m. More detailed descriptions are presented in the published literature (Tang et al. 2016; Zhu et al. 2016). In this study, the gradient method (Steyn et al. 1999) is used to determine the MLH; that is, the top of the mixing layer was determined by the maximum negative gradient value in the profile of the atmosphere backscattering coefficient. Moreover, to eliminate the interference of the aerosol layer structure and the detection noise, the MLH was calculated by the improved gradient method after smoothly averaging the profile data (Münkel et al. 2007; Tang et al. 2015).

Doppler wind radar uses the remote sensing method of laser detection and ranging technology and measures the Doppler frequency shift generated by the laser through the backscatter echo signal of particles in the air. The Windcube 100s can provide 3D wind field data within a 3 km range from the system, including u, v and w vectors. In the actual measurement, starting from 100 m, the spatial resolution is 50 m, the WS accuracy is < 0.5 m s^{-1}, and the radial WS range is -30 m s^{-1} to 30 m s^{-1}.

2.3 Other data

During the observations, the hourly PM$_{2.5}$ concentrations of the Beijing Olympic Sports Center (39.99° N, 116.40° W) were obtained from the Ministry of Environmental Protection of China (http://www.zhb.gov.cn/).

2.4 Analytical method

The atmospheric dilution is composed of vertical and horizontal dilution, which can be characterized by the MLH and wind speed in the mixing layer (WS$_{ML}$), respectively. The VC (m^2 s^{-1}) was obtained by combining the MLH (m) and WS$_{ML}$ (m s^{-1}) and can be used for a comprehensive evaluation of the vertical and horizontal dilutions. Higher dilution-related parameters (MLH, WS$_{ML}$ and VC) indicate a stronger dilution capability, which is conducive to the transport and dilution of heavy air pollution.

The VC calculation method is as follows:

$$VC = H_{ML} \times WS_{ML}, \tag{1}$$

$$WS_{ML} = \frac{1}{n} \sum_{i=1}^{n} WS_i, \tag{2}$$

138 $$WS_i = \sqrt{\overline{u_i}^2 + \overline{v_i}^2},\tag{3}$$

139 where WS_{ML} is the average WS within the mixing layer, calculated by Eq. (2); H_{ML} is the height of
140 the mixing layer; WS_i is the WS observed at a certain height, calculated by u_i and v_i in the wind
141 profile according to Eq. (3); and n is the number of measurement layers in the mixing layer (Nair et
142 al. 2007).
143 The TF (mg m^{-2}s^{-1}) is determined by the WS and the PM$_{2.5}$ concentration in the area under analysis.
144 The calculation method for a certain height is shown in Eq. (4):

145 $$TF_{u_i} = u_i \times C_i,\tag{4}$$

146 where C_i is the concentration of PM$_{2.5}$ at a certain height. However, it is extremely difficult to
147 observe the vertical PM$_{2.5}$ concentration in the mixing layer. To obtain the PM$_{2.5}$ concentration
148 profile, we studied the backscattering coefficient measured by ceilometer, and found that the
149 concentration of near-surface PM$_{2.5}$ is strongly correlated with the backscattering coefficient at 100
150 m (Fig. S1). Thus, based on the relationship between the two, the backscattering coefficient profile
151 can be used to invert the vertical PM$_{2.5}$ concentration profile. Then, the TFs in the mixing layer are
152 calculated as follows:

153 $$TF_u = \int_{i=1}^{n} (u_i \times C_i)$$

154 $$TF_v = \int_{i=1}^{n} (v_i \times C_i)\tag{5}$$

155 Through the above method, radial and zonal TFs can be obtained, and vector synthesis in two
156 directions can be conducted to obtain the main transport direction to find the transport source area.

157 **3. Results and discussion**

158 **3.1 Boundary layer meteorology**

159 **3.1.1 Seasonal variation**

160 To understand the variations of the atmospheric dilution capability, we carried out continuous
161 measurements of the MLH and wind profile within the mixing layer over a 2-year period (2016.1.1-
162 2017.12.31). The availability was verified after MLH elimination by Tang et al. (Tang et al. 2016).
163 After the exclusion of the data of the MLH under rainy, sandstorm and windy conditions, the data
164 availability was 95% over the 2-year period, higher than that of previous studies (Mues et al. 2017;
165 Tang et al. 2016). The availability was the lowest in February, at 86%, and the highest in July, at
166 99%.
167 In terms of the seasonal variation, the average MLHs for the spring (781 ± 229 m) (value $\pm$ standard
168 deviation) and summer (767 ± 219 m) were higher than those of the autumn (612 ± 166 m) and
169 winter (584 ± 221 m) (Fig. 1). However, WS_{ML} was different from the MLH in terms of the seasonal
170 variation, with the largest value 4.6 ± 1.6 m s^{-1} in the spring, followed by the winter (4.1 ± 2.7 m s^{-1})
171 and autumn (3.7 ± 1.6 m s^{-1}), and the smallest value 3.6 ± 1.1 m s^{-1} in the summer. The VC was
172 calculated by the MLH and wind profile, and the results demonstrate that the dilution capability was
173 strongest in the spring, as the VC reached as high as 3940 ± 2110 m^2 s^{-1}. The atmospheric dilution
174 capabilities for the summer, winter and autumn were similar, with VC values of 2953 ± 1322 m^2 s^{-}

175 ¹, 2913 ± 3323 m² s⁻¹ and 2580 ± 1601 m² s⁻¹, respectively. A monthly analysis shows that the
176 atmospheric dilution capability was strongest in May, when the VC was as high as 5161 ± 2085 m²
177 s⁻¹, and worst in December, when the VC was only 1690 ± 1072 m² s⁻¹. The VC value in May was
178 3.1 times that in December. To analyze the impact of the dilution capacity on $PM_{2.5}$, the seasonal
179 variation of $PM_{2.5}$ was analyzed. The average $PM_{2.5}$ concentration for the winter (80 ± 87 µg m⁻³)
180 was the highest, followed by autumn (68 ± 54 µg m⁻³) and spring (67 ± 60 µg m⁻³), and that of the
181 summer (51 ± 29 µg m⁻³) was the lowest. The lowest monthly average $PM_{2.5}$ concentration was 42
182 ± 26 µg m⁻³ in August. The highest monthly average was in January at 94 ± 100 µg m⁻³, 2.2 times
183 that in August (Fig. 1).
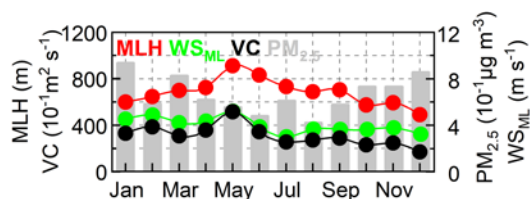
185 Fig. 1 Monthly variations in mixing layer height (MLH), the wind speed in the mixing layer
186 (WS_{ML}), the ventilation coefficient (VC) and $PM_{2.5}$ in Beijing.

187 Although there is little difference in the dilution capability between the summer, autumn and winter,
188 there is serious pollution in the autumn and winter. To analyze this problem, the VC frequency
189 distribution was studied. The results show that the VC had a high frequency in the range of 1000-
190 4000 m² s⁻¹ from 2016 to 2017, but the frequency distribution was different in different seasons (Fig.
191 2). The VC showed a strong dilution capability in the spring, mainly in the range of 2000-5000 m²
192 s⁻¹, with the highest frequency (24%) in the range of 2000-3000 m² s⁻¹. In the summer, the high
193 frequency of the VC occurred in the range of 1000-4000 m² s⁻¹, which was slightly lower than that
194 in the spring, and the highest frequency (27%) occurred in the range of 3000-4000 m² s⁻¹.
195 Additionally, the VC high frequency appeared in lower ranges in the autumn and winter. The VC
196 occurred at a high frequency of 1000-3000 m² s⁻¹ in the autumn, and the highest frequency occurred
197 within the range of 2000-3000 m² s⁻¹, accounting for 33%. In the winter, the VC appeared more
198 frequently in the range of 0-2000 m² s⁻¹ and was the highest in the range of 1000-2000 m² s⁻¹, which
199 was 28%. In the winter, when the Siberian High transits, strong northwest winds prevail in the
200 Beijing area (Fig. 5), resulting in the higher frequency of the VC in the range of 1000-2000 m² s⁻¹.
201 The VC frequency of 0-1000 m² s⁻¹ in the winter was significantly higher than that of the other
202 seasons, up to 22%, which was 7 times that in the spring, 5 times that in the summer and 2 times
203 that in the autumn. According to the seasonal variation in the $PM_{2.5}$ concentration, heavy pollution
204 in the autumn and winter is related to the high frequency of poor atmospheric dilution capability.
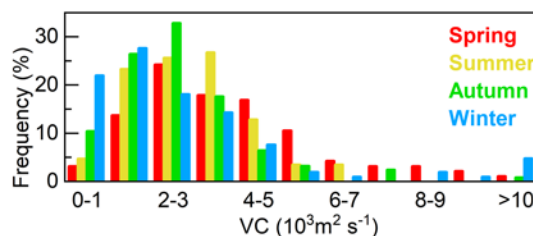
206 Fig. 2 Frequency distribution of the daily VC from January 2016 to December 2017 in Beijing.

3.1.2 Diurnal variation

Moreover, the diurnal variations in the dilution-related parameters during different seasons were analyzed to reveal the diurnal evolution of the atmospheric dilution capability. The peak and trough values of the MLH and VC appeared simultaneously at approximately 15:30 LT and 05:30 LT, respectively. Generally, the daily variation in the MLH is characterized by a low value at night, which increases rapidly after sunrise and reaches the maximum value in the afternoon (Fig. 3a). The daily maximum value of the MLH is seasonal, where it is higher in the spring and summer and lower in the autumn and winter. The daily minimum value of the MLH generally occurs when the mixing layer is stable and is closely related to the WS. The diurnal variation in WS_{ML} is smaller, with a peak at approximately 19:30 LT and a trough at approximately 10:00 LT, which are ~4 h later than the peak and trough of the MLH (Fig. 3b). The diurnal variation in the VC is similar to that of the MLH, showing that the dilution capability is strong before sunset, gradually weakens after sunset and remains stable at night. The dilution capability in the spring was significantly stronger than that during the other seasons, and the maximum daily value reached 8678 m^2 s^{-1} (Fig. 3c). The daily maximum values of the VC in the summer, autumn and winter were close, at approximately 5000 m^2 s^{-1} (Fig. 3c). The VC growth rate in the spring was significantly higher than that in the other seasons, reaching a maximum at approximately 09:00 LT. In the autumn, the VC growth rate peaked at approximately 10:00 LT, and those in the summer and winter peaked at approximately 11:00 LT. Throughout the year, the VC began to increase during the winter later than in other seasons, at approximately 09:00 LT, indicating that the weaker dilution capability remained for a longer period during the winter. The VC was weakened most rapidly in the spring; however, it was still higher than that of the other seasons after declining. In addition to the spring, the VC in the autumn and winter weakened the most rapidly, and the most slowly in the summer. In general, the vertical and horizontal dilutions are strong in the spring during both the day and night. In the winter, the vertical dilution is weak during the day, and the horizontal dilution during the night is the main component. In the summer, the vertical dilution during the day is dominant.

Notable differences are present when we compare the dilution-related parameters to the $PM_{2.5}$ concentration. The daily maximum $PM_{2.5}$ concentrations in the spring, summer, autumn and winter were 73 µg m^{-3} (11:00 LT), 56 µg m^{-3} (09:00 LT), 78 µg m^{-3} (23:00 LT) and 101 µg m^{-3} (01:00 LT), respectively. The differences between the maximum and minimum were 14 µg m^{-3}, 10 µg m^{-3}, 20 µg m^{-3} and 38 µg m^{-3}, respectively. Thus, the diurnal variation of $PM_{2.5}$ can be divided into two categories: (1) the highest value occurs in the midday in the spring and summer and the overall change is small, and (2) the highest value occurs during the night in the autumn and winter and differs greatly from the lowest value (Fig. 3d). The main causes of air pollution are local emissions and regional transportation. Thus, these results indicate that there are greater local contributions in the autumn and winter and higher regional transport in the spring and summer.
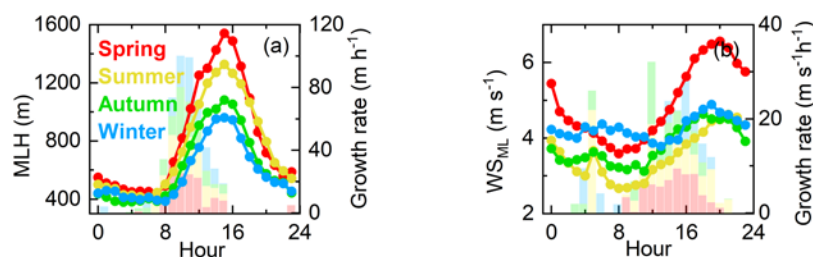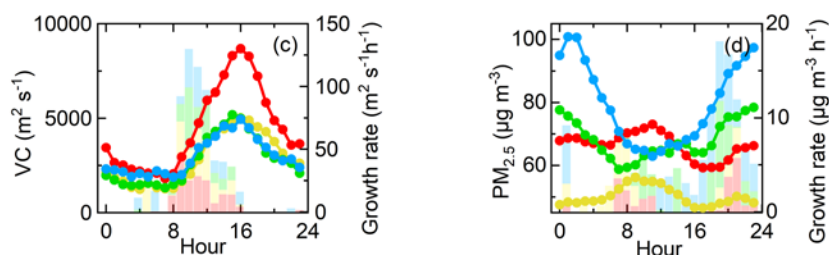
244

245   Fig. 3 Diurnal variations and growth rates of MLH (a), WS_{ML} (b), VC (c) and $PM_{2.5}$ (d) in the

246   spring, summer, autumn and winter in Beijing. Diurnal variations are represented by lines and

247   scatters. Growth rates are represented by columns, and only positive values are shown in the

248   figure.

249   **3.2 Mixing layer TF of $PM_{2.5}$**

250   **3.2.1 Temporal evolution of TF**

251   To quantify the transport of $PM_{2.5}$ in Beijing, the transport direction of $PM_{2.5}$ was characterized by

252   the average wind direction in the mixing layer. As shown in Fig. 4, the mixing layer TF in the spring

253   was the largest, reaching 4.33 ± 0.69 mg m^{-1}s^{-1}, and there was no significant difference in the

254   summer, autumn or winter, when the TF values were 2.27 ± 0.42 mg m^{-1}s^{-1}, 2.39 ± 0.45 mg m^{-1}s^{-1}

255   and 2.89 ± 0.49 mg m^{-1}s^{-1}, respectively. The transport sources of the cold period in Beijing were

256   predominantly from the northwesterly and westerly directions. With temperature warming, the

257   transport direction gradually changed from west to south, mainly southwesterly in the spring and

258   southerly in the summer. The monthly average maximum value of the TF occurred in May, as high

259   as 5.00 ± 5.21 mg m^{-1}s^{-1} and mainly originated from the southwest direction, accompanied by a

260   strong wind. The minimum value appeared in August, as low as 1.70 ± 1.73 mg m^{-1}s^{-1}, which was

261   mainly transported from western regions, with a small WS. The TF in May was 3 times that in

262   August (Fig. 4). Therefore, the change in the transport direction leads to an obvious seasonal

263   variation in the TF. Overall, the regional transport contributes the most to the $PM_{2.5}$ concentration

264   in the spring, which is mainly related to increased dust activities; regional transport has a smaller

265   contribution in the winter, but there is a high near-surface $PM_{2.5}$ concentration, which indicates that

266   more focus should be given to local emission source control; in the summer and autumn, the

267   southwest airflow transport influence on the Beijing should receive more focus.
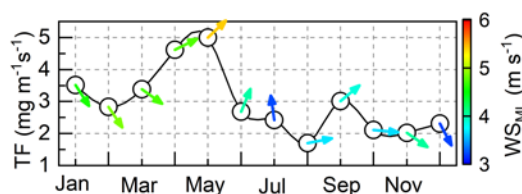
268

269   Fig. 4 Seasonal variations in the mixing layer TF of $PM_{2.5}$ and the transport direction.

270   To understand the regional transport influence on the Beijing area, the diurnal variations of the

271   mixing layer TF were analyzed during different seasons in Beijing. The daily minimum value of the

272   TF appeared at approximately 07:00 LT and was accompanied by a northerly wind. As the average

273 wind direction in the mixing layer gradually turned south, the daily minimum value of the TF
274 continued to rise until the daily maximum value appeared at approximately 16:00 LT (Fig. 5).
275 Transport mainly occurred between 14:00 and 18:00 LT, which was consistent with the results of a
276 previous study (Ge et al. 2018). In the spring, the WS was the highest, so the peak TF duration was
277 the shortest; it peaked at only 16:00 LT (9.50 mg $m^{-1}s^{-1}$) and then dropped sharply to 1.94 mg $m^{-1}s^{-1}$
278 ^{1}. Therefore, the diurnal variation in the TF during the spring showed the characteristics of a rapid
279 rise and rapid decline. The peak duration was approximately 3 h for a long time in the summer and
280 autumn, where the daily maximum values were 3.79 mg $m^{-1}s^{-1}$ and 3.63 mg $m^{-1}s^{-1}$ and the minimum
281 values were 1.00 mg $m^{-1}s^{-1}$ and 1.30 mg $m^{-1}s^{-1}$, respectively. The diurnal variation in the TF during
282 the summer and autumn showed the characteristics of a slow rise and slow decline. Specifically, the
283 daily variation had a strong fluctuation in the winter, peaked three times at 14:00 LT (4.06 mg $m^{-1}s^{-1}$
284 ^{1}), 16:00 LT (4.38 mg $m^{-1}s^{-1}$) and 19:00 LT (4.07 mg $m^{-1}s^{-1}$), then dropped slowly to 1.66 mg $m^{-1}s^{-1}$
285 ^{1}. Another special point is that in the spring, summer and autumn, a high TF corresponds to a
286 southerly wind, while in the winter, the southerly wind does not appear in the whole transport
287 process; instead, there is a westerly wind, which is influenced by the Siberian High.
288 Even so, the TF variation patterns can be summarized as that a high TF corresponds to a southerly
289 wind and a low TF corresponds to a northerly wind (Fig. 5). When the average wind direction in the
290 mixing layer changes from north to south, the TF gradually increases from the daily minimum to
291 the daily maximum. The TF increased by 5 times in the spring, 4 times in the summer, and 3 times
292 in the autumn and winter. The current pattern is because areas located in the south of Beijing are
293 heavily polluted and southerly winds help transport pollutants into the city, leading to high TFs in
294 the afternoons (Fig. 5). However, due to the high mixing layer in the spring, the concentration of
295 near-surface $PM_{2.5}$ did not increase. The results further confirm the conclusion that the northwest
296 wind in Beijing is a clean wind (Wang et al. 2015; Zhang et al. 2018). Thus, the northwest wind is
297 conducive to the outward transport of pollutants from Beijing, which helps to alleviate pollution. As
298 a result, there was no high TF in the winter when the northwest wind prevailed. On the other hand,
299 southerly winds are stronger than northerly winds (Fig. 5), which can also result in a high TF.
300 Therefore, the level of the TF is determined by two factors, the WS and $PM_{2.5}$ concentration. In the
301 spring, summer and autumn, a strong south wind prevails in the afternoon. As the south wind is
302 often accompanied by high $PM_{2.5}$ concentrations (Fig. S2), the TF is high. In the winter, the whole
303 day is dominated by westerly and northerly winds. Although the northerly winds are strong, the TF
304 is not high due to the low $PM_{2.5}$ concentration. Generally, a high WS means fast mixing, and the
305 corresponding MLH is also high. At this time, the TF is mainly controlled by the WS. While the WS
306 is low, the mixing speed is slow and the MLH is low. At this time, the TF is mainly controlled by
307 $PM_{2.5}$ concentration. From the above analysis, it can be inferred that if the MLH and WS gradually
308 decrease with the worsening of the pollution, the mixing layer TF is controlled by the WS first and
309 then by the $PM_{2.5}$ concentration, a maximum TF may occur at a critical moment. This moment is
310 neither the moment of the maximum WS nor the moment of the maximum $PM_{2.5}$ concentration but
311 rather should be somewhere in between. This will be discussed in more detail in section 3.3.
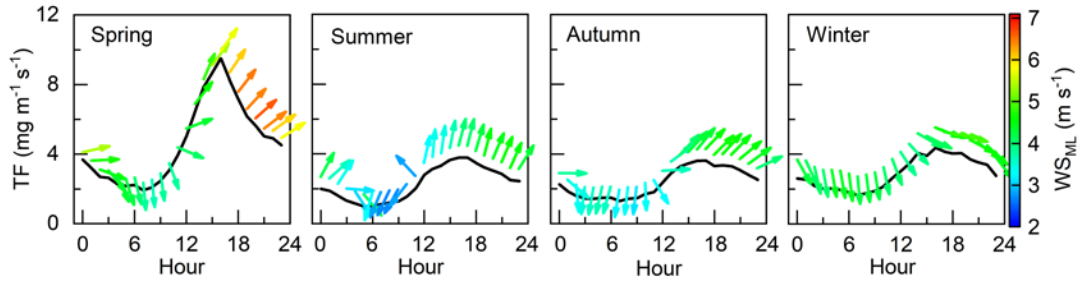
Fig. 5 Diurnal variations in the mixing layer TF of PM$_{2.5}$ and transport direction during different seasons in Beijing.

3.2.2 Vertical evolution of TF

After the aforementioned analyses, the transport period is known. To further explore the height of transport, we studied the seasonal variation of the TF profile in combination with the vertical wind and PM$_{2.5}$ profiles. With the increasing altitude, the WS first increases sharply at approximately 200 m and then slowly increases, and the differences between different seasons gradually become significant. The WS is always smallest in the summer and strongest in the winter. It is the same in the spring and autumn at 1200 m. Above 1200 m, the WS in the autumn exceeds that in the spring. The PM$_{2.5}$ concentration at 100 m obtained by inversion is highest in the winter (93.7 mg m^{-2}s^{-1}), similar in the spring and autumn (80.3 mg m^{-2}s^{-1} and 75.8 mg m^{-2}s^{-1}, respectively), and lowest in the summer (53.5 mg m^{-2}s^{-1}). This finding is consistent with the near-surface results. Below 200 m, the PM$_{2.5}$ concentration is relatively uniform. As the height increases, the PM$_{2.5}$ concentration decreases gradually. Between 200-600 m, the PM$_{2.5}$ concentration begins to decrease rapidly, but the rate of decline is obviously different in different seasons. In the autumn and winter, the reduction rate of the PM$_{2.5}$ concentration is significantly higher than that in the spring and summer. As a result, the spring PM$_{2.5}$ concentration at 400 m begins to be greater than that in the winter; the summer PM$_{2.5}$ concentration at 650 m begins to be greater than that in the autumn and is at the same level as that in the winter. Over 600 m, there is no significant difference in the PM$_{2.5}$ concentration between different seasons, while the WS varies greatly. Therefore, the TF is greatly affected by the WS at high altitudes, and it is greatly influenced by the PM$_{2.5}$ concentration near the ground. The TF in the mixing layer is also affected by the MLH.

The vertical evolution of the TF is different from both the evolution of the WS and PM$_{2.5}$ concentration, and the seasonal variation remains consistent from the near-surface to the upper air. The TF for the spring is the highest, followed by the winter and autumn, and that of the summer is the lowest. The vertical variation in the TF increases first and then decreases, and a peak appears at approximately 300 m, with a value of 0.38 mg m^{-2}s^{-1} in the spring, 0.19 mg m^{-2}s^{-1} in the summer, 0.24 mg m^{-2}s^{-1} in the autumn, and 0.31 mg m^{-2}s^{-1} in the winter. In the process of the TF lowering, it has different performances in different seasons. In the spring, the decline slows down at approximately 1500 m. The changes in the summer and autumn are similar. After the peak, the TF drops rapidly in the summer and autumn. The decrease rate above 500 m becomes slow, slows down again after 1500 m, and finally the profiles become vertical. In the winter, the TF declines rapidly, followed by fluctuations at approximately 1000 m. The above results preliminarily indicate that the transport mainly occurs within 200-1500 m, which will be evaluated in Sec. 3.3. To sum up, in the

347 autumn and winter, the high concentration of $PM_{2.5}$ is concentrated near the ground, while the TF is
348 not large, again indicating that local emissions are the main source of $PM_{2.5}$ in the autumn and winter;
349 in the spring, affected by high-altitude transport, the $PM_{2.5}$ concentration is high; and in the summer,
350 both the TF and $PM_{2.5}$ concentration are at their lowest levels, indicating that regional transport may
351 play an important role in the $PM_{2.5}$ concentration in the summer.
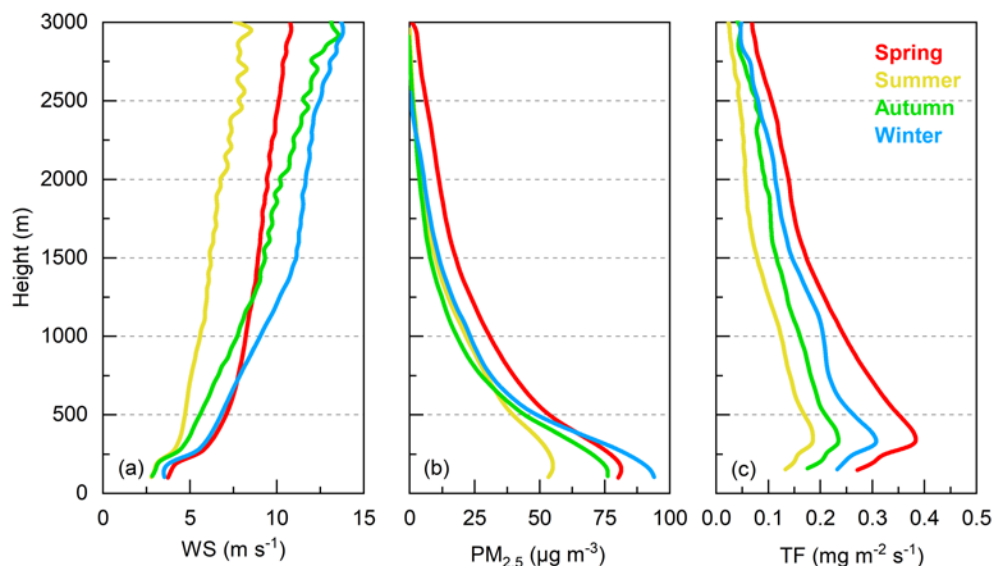
352
353   Fig. 6 Vertical profiles of WS (a), $PM_{2.5}$ (b) and TF of $PM_{2.5}$ (c) in different seasons in Beijing.

354 **3.3 TF under different degrees of air pollution**

355 Previous studies have demonstrated that transport occurs only in the transition period of pollution,
356 while it is weak at the peak of pollution (Tang et al. 2015; Zhu et al. 2016). To quantify the transport
357 impact of different pollution levels, the $PM_{2.5}$ concentration was divided into five levels according
358 to the "Technical Regulation on Ambient Air Quality Index (on trial)" (HJ 633-2012): $PM_{2.5} \leq$
359 35 µg m^{-3} (clear days), $35 < PM_{2.5} \leq 75$ µg m^{-3} (slight pollution), $75 < PM_{2.5} \leq 115$ µg m^{-3} (light
360 pollution), $115 < PM_{2.5} \leq 150$ µg m^{-3} (medium pollution) and $PM_{2.5} > 150$ µg m^{-3} (heavy pollution).
361 An interesting phenomenon is that with the increase in altitude, the heavier the pollution near the
362 ground is, the greater the reduction rate of the $PM_{2.5}$ concentration is (Fig. 7). As a result, there is a
363 reversal at 1000-1500 m. In other words, the more severe the near-surface pollution, the lower the
364 high-altitude $PM_{2.5}$ concentration. This is particularly outstanding in the spring: from a clear to a
365 heavy polluted day, the TF at 100 m was, in turn, 0.15 mg m^{-2}s^{-1}, 0.26 mg m^{-2}s^{-1}, 0.32 mg m^{-2}s^{-1},
366 0.39 mg m^{-2}s^{-1}, 0.66 mg m^{-2}s^{-1}, and at 2600 m, the values dropped to 0.15 mg m^{-2}s^{-1}, 0.17 mg m^{-2}s^{-1},
367 0.13 mg m^{-2}s^{-1}, 0.10 mg m^{-2}s^{-1} and 0.07 mg m^{-2}s^{-1}, respectively. That is, the lower the pollution
368 degree, the more vertical the TF tends to be. This is related to the MLH, because a high MLH is
369 conducive to the diffusion of pollutants in the vertical direction. With the worsening of pollution,
370 the MLH shows a downward trend (Fig. S3).
371 According to the previous analysis, two peaks may appear in the TF profile, indicating that the
372 transport occurs at two different heights, approximately 200 m (low-altitude transport) and 1000 m
373 (high-altitude transport), respectively. Due to the sudden increase in the WS at approximately 200
374 m, the low-altitude transport at 200 m is the basic transport height, regardless of the season and the
375 degree of pollution. In contrast, the high-altitude transport is quite special and mainly occurs in the

winter when there is significant pollution. A small peak of in the TF can also be found on heavy polluted days in the summer. Although the change in the TF profile of medium pollution in the autumn is not as obvious as that in the summer and winter, a small increase can still be seen (Fig. 7). In the case of heavy pollution, the MLH is usually less than 1000 m, while in the case of clear and slight pollution, the MLH is close to the height of high-altitude transport (Fig. S3). Therefore, it can be inferred that the pollutants transported at a high altitude during heavy pollution are stored in the residual layer, and when the mixing layer becomes higher, the pollutants stored in the residual layer diffuse into the mixing layer, affecting the pollution level within the mixing layer. This may be a key contributor to the slight pollution in the summer, autumn and winter, but further research is needed.
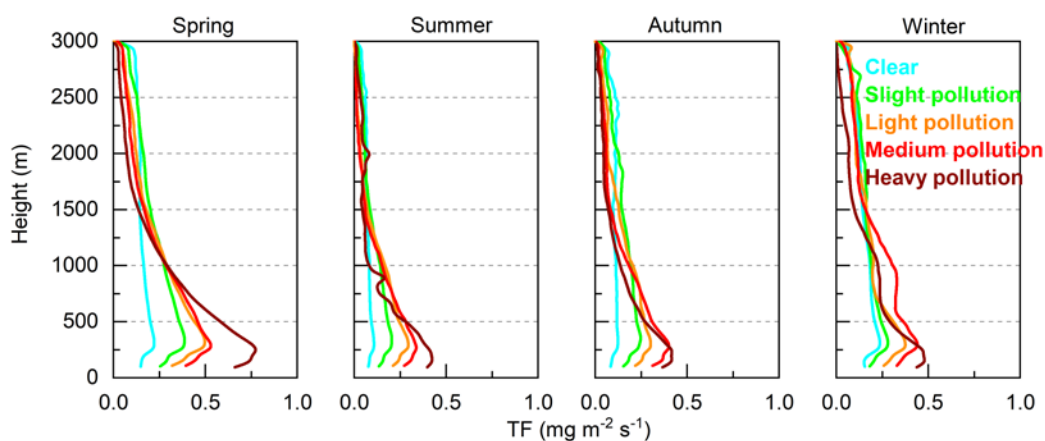
Fig. 7 Vertical profiles of TF of $PM_{2.5}$ under different degrees of pollution in different seasons in Beijing. Clear days: $PM_{2.5} \leq 35$ μg m^{-3}, slight pollution: $35 < PM_{2.5} \leq 75$ μg m^{-3}, light pollution: $75 < PM_{2.5} \leq 115$ μg m^{-3}, medium pollution: $115 < PM_{2.5} \leq 150$ μg m^{-3} and heavy pollution: $PM_{2.5} > 150$ μg m^{-3}.

According to the same division method, we further explored the seasonal variation of the TF and transport source in the mixing layer under different pollution degrees. With pollution aggravation, the mixing layer TF in Beijing increased by varying degrees during different seasons, and the transport direction gradually shifted from northwest to south (except during the winter) (Fig. 8). In particular, the mixing layer TF in the spring is significantly higher than that in the other seasons at all pollution degrees, which is 1.1-2.0 times that in the other seasons. This may be caused by the greater amount of dust during the spring. With the pollution deterioration, the TF showed an increasing trend in the initial stage of pollution and a decreasing trend during the heavy pollution period. From medium pollution to heavy pollution, the TF decreased from 5.50 ± 4.83 mg m^{-1}s^{-1} to 4.69 ± 4.84 mg m^{-1}s^{-1}in the spring, from 3.94 ± 2.36 mg m^{-1}s^{-1} to 3.39 ± 1.77 mg m^{-1}s^{-1} in the summer, from 3.72 ± 2.86 mg m^{-1}s^{-1} to 3.01 ± 2.40 mg m^{-1}s^{-1} in the autumn, and from 4.45 ± 4.40 mg m^{-1}s^{-1} to 3.25 ± 2.77 mg m^{-1}s^{-1} in the winter. Among them, the largest drop was found in the winter. In the winter, with the pollution aggravation, the transport direction changed from northwest to southwest and finally to the north. In contrast to in the other seasons, the weak north wind was the main wind during heavy pollution in the winter, indicating that regional transport contributed less to the heavy pollution during the winter in Beijing. In the initial stage of pollution, the TF continued to increase, but the rate of increase gradually slowed in the spring and summer. From light pollution to medium pollution, the TF decreased by 0.1mg m^{-1}s^{-1} in the spring and increased by only 0.07 mg m^{-1}s^{-1} in the summer. It is also not difficult to find from the changes in the TF profile (Fig. 7) that the regional

transport has little impact on the medium pollution in the spring and summer. These results indicate that although the region south of Beijing is the main transport source in Beijing, its contribution is significantly reduced during the severe pollution period. In general, regional transport plays an important role in the initial period of pollution, while local emissions are the main controlling factor during the period of heavy pollution. The parabolic pattern of the TF is the result of a combination of the WS and $PM_{2.5}$ concentration. The TF reaches a threshold during medium pollution, which is the critical moment mentioned above.
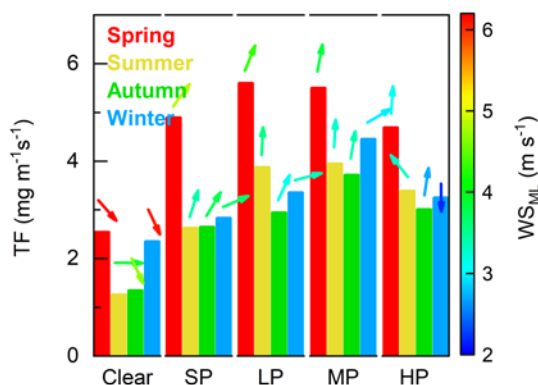
Fig. 8 The mixing layer TF of the $PM_{2.5}$ levels and transport directions under different degrees of pollution in different seasons in Beijing. (SP denotes slight pollution, LP denotes light pollution, MP denotes medium pollution and HP denotes heavy pollution.)

4. Conclusions

To understand the characteristics of the $PM_{2.5}$ transport flux in Beijing, the height of the atmospheric mixing layer and the wind profile within the mixing layer in Beijing were observed for a 2-year period. The main conclusions are as follows:

(1) By analyzing the variations in the VC, it is found that the atmospheric dilution capability in Beijing is strongest in the spring and weaker in the summer, autumn and winter. In the spring, the vertical and horizontal dilution capacities are strong; in the autumn and winter, the vertical and horizontal dilution capacities are weak; and in the summer, the vertical dilution capability is strong and the horizontal dilution capability is weak. The diurnal variation in the VC is consistent with the MLH, which shows that the dilution capability is the strongest before sunset, gradually weakens after sunset and remains stable at night. In the spring, the vertical and horizontal dilutions are strong during both day and night. In the winter, the vertical dilution is weak during the day, and the horizontal dilution during the night is the main component. In the summer, the vertical dilution during the day is dominant. Although there is little difference in the diffusivity between the summer, autumn and winter, the poor dilution capability occurs more frequently in the autumn and winter.

(2) The TF is the largest in the spring and smaller in the summer, autumn and winter in Beijing. The high TF mainly comes from southward transport, while the low TF is accompanied by northwest transport. The transport mainly occurred between 14:00 and 18:00 LT, and the height of the transport is at approximately 200 m and 1000 m. Using the $PM_{2.5}$ concentration as a classification index for the air pollution, the results show that the regional transport from the southern area plays an important role in the initial period of pollution, and local emissions are the main controlling factors

in the heavy pollution period, especially in the winter.

To solve the problem of heavy pollution in northern China, joint prevention and control has been suggested for a long time. Even so, there is still no concrete implementation plan. To break through this embarrassing situation, this study quantifies TF to explain the time period when the transport occurs and the main areas affected in Beijing. In this study, the atmospheric dilution capability during different seasons and the TF during different pollution periods were also discussed. The important role of transport in the initial period of pollution is emphasized, and local pollutant emission control is found to be the most effective way of mitigating pollution levels. The research results are of great significance to the early warning, prevention and control of atmospheric particulate pollution.

Data availability

The data in this study are available from the corresponding author upon request (tgq@dq.cern.ac.cn).

Author contribution

GT and YW designed the research, LZ, BH, BL and YunL conducted the measurements. YusL and GT wrote the paper. SL reviewed and commented on the paper.

Competing interests

The authors declare that they have no conflicts of interest to disclose.

Acknowledgments

This work was supported by the National Key R&D Program of China (2018YFC0213201), the Young Talent Project of the Center for Excellence in Regional Atmospheric Environment CAS (CERAE201802), LAC/CMA (2017A01), the National Research Program for Key Issues in Air Pollution Control (DQGG0101), the National Natural Science Foundation of China (Nos. 41705113 and 41877312), and the Foundation of the Chinese Academy of Meteorological Sciences (2019Y001).

References

Chang, X., S. Wang, B. Zhao, S. Cai, and J. Hao: Assessment of inter-city transport of particulate matter in the Beijing–Tianjin–Hebei region, Atmos. Chem. Phys., 18, 4843-4858, doi: 10.5194/acp-18-4843-2018, 2018.

Cheng, J., J. Su, T. Cui, X. Li, X. Dong, F. Sun, Y. Yang, D. Tong, Y. Zheng, J. Li, Q. Zhang, and K. He: Dominant role of emission reduction in PM2.5 air quality improvement in Beijing during 2013-2017: a model-based decomposition analysis, Atmos. Chem. Phys. Discussions, 1-31, doi: 10.5194/acp-2018-1145, 2018a.

Cheng, N., Y. Li, B. Cheng, X. Wang, F. Meng, Q. Wang, and Q. Qiu: Comparisons of two serious air pollution episodes in winter and summer in Beijing, J. Environ. Sci-China., 69, 141-154, doi:

10.1016/j.jes.2017.10.002, 2018b.

Ge, B., Z. Wang, W. Lin, X. Xu, J. Li, D. Ji, and Z. Ma: Air pollution over the North China Plain and its implication of regional transport: A new sight from the observed evidences, Environ. Pollut., 234, 29-38, doi: 10.1016/j.envpol.2017.10.084, 2018.

Geiß, A., M. Wiegner, B. Bonn, K. Schäfer, R. Forkel, E. von Schneidemesser, C. Münkel, K. L. Chan, and R. Nothard: Mixing layer height as an indicator for urban air quality?, Atmos. Meas. Tech., 10, 2969-2988, doi: 10.5194/amt-10-2969-2017, 2017.

Huang, Q., X. Cai, J. Wang, Y. Song, and T. Zhu: Climatological study of the boundary-layer air stagnation Index for China and its relationship with air pollution, Atmos. Chem. Phys., 18, 7573-7593, doi: 10.5194/acp-18-7573-2018, 2018.

Li, H., F. Duan, Y. Ma, K. He, L. Zhu, T. Ma, S. Ye, S. Yang, T. Huang, and T. Kimoto: Case study of spring haze in Beijing: Characteristics, formation processes, secondary transition, and regional transportation, Environ. Pollut., 242, 544-554, doi: 10.1016/j.envpol.2018.07.001, 2018.

Liu, L., J. Guo, Y. Miao, L. Liu, J. Li, D. Chen, J. He, and C. Cui: Elucidating the relationship between aerosol concentration and summertime boundary layer structure in central China, Environ. Pollut., 241, 646-653, doi: 10.1016/j.envpol.2018.06.008, 2018.

Miao, Y., and S. Liu: Linkages between aerosol pollution and planetary boundary layer structure in China, Sci. Total. Environ, 650, 288-296, doi: 10.1016/j.scitotenv.2018.09.032, 2019.

Mues, A., M. Rupakheti, C. Münkel, A. Lauer, H. Bozem, P. Hoor, T. Butler, and M. G. Lawrence: Investigation of the mixing layer height derived from ceilometer measurements in the Kathmandu Valley and implications for local air quality, Atmos. Chem. Phys., 17, 8157-8176, doi: 10.5194/acp-17-8157-2017, 2017.

Münkel, C., N. Eresmaa, J. Räsänen, and A. Karppinene: Retrieval of mixing height and dust concentration with lidar ceilometer, Bound-Lay. Meteorol, 124, 117-128, doi: 10.1007/s10546-006-9103-3, 2007.

Nair, V. S., K. K. Moorthy, D. P. Alappattu, P. K. Kunhikrishnan, S. George, P. R. Nair, S. S. Babu, B. Abish, S. K. Satheesh, S. N. Tripathi, K. Niranjan, B. L. Madhavan, V. Srikant, C. B. S. Dutt, K. V. S. Badarinath, and R. R. Reddy: Wintertime aerosol characteristics over the Indo-Gangetic Plain (IGP): Impacts of local boundary layer processes and long-range transport, J. Geophys. Res-Atmos., 112, D13205, doi: 10.1029/2006jd008099, 2007.

Ouyang, W., Y. Xu, J. Cao, X. Gao, B. Gao, Z. Hao, and C. Lin: Rainwater characteristics and interaction with atmospheric particle matter transportation analyzed by remote sensing around Beijing, Sci. Total Environ., 651, 532-540, doi: 10.1016/j.scitotenv.2018.09.120, 2019.

Schäfer, K., S. Emeis, H. Hoffmann, and C. Jahn: Influence of mixing layer height upon air pollution in urban and sub-urban areas, Meteorol. Z., 15, 647-658, doi: 10.1127/0941-2948/2006/0164, 2006.

Shen, Y., L. Zhang, X. Fang, H. Ji, X. Li, and Z. Zhao: Spatiotemporal patterns of recent PM2.5 concentrations over typical urban agglomerations in China, Sci Total Environ, 655, 13-26, doi: 10.1016/j.scitotenv.2018.11.105, 2019.

Song, L. C., G. Rong, L. Ying, and W. Guo-Fu: Analysis of China's haze days in the winter half-year and the climatic background during 1961–2012, Advances in Climate Change Research, 5, 1-6, doi: 10.3724/sp.j.1248.2014.001, 2014.

Steyn, D. G., M. Baldi, and R. M. Hoff: The detection of mixed layer depth and entrainment zone thickness from lidar backscatter profiles, J. Atmos. Ocean. Technol., 16, 953-959, doi, 1999.

Su, T., Z. Li, and R. Kahn: Relationships between the planetary boundary layer height and surface pollutants derived from lidar observations over China, Atmos. Chem. Phys., 18, 15921-15935, doi: 10.5194/acp-18-15921-2018, 2018.

Tang, G., J. Zhang, X. Zhu, T. Song, C. Münkel, B. Hu, K. Schäfer, Z. Liu, J. Zhang, L. Wang, J. Xin, P. Suppan, and Y. Wang: Mixing layer height and its implications for air pollution over Beijing, China, Atmos. Chem. Phys., 16, 2459-2475, doi: 10.5194/acp-16-2459-2016, 2016.

Tang, G., X. Zhu, B. Hu, J. Xin, L. Wang, C. Munkel, G. Mao, and Y. Wang: Impact of emission controls on air quality in Beijing during APEC 2014: lidar ceilometer observations, Atmos. Chem. Phys., 15, 12667-12680, doi: 10.5194/acp-15-12667-2015, 2015.

Wang, L., Z. Liu, Y. Sun, D. Ji, and Y. Wang: Long-range transport and regional sources of PM2.5 in Beijing based on long-term observations from 2005 to 2010, Atmos. Res., 37-48, doi: 10.1016/j.atmosres.2014.12.003, 2015.

Wang, X., K. Wang, and L. Su: Contribution of Atmospheric Diffusion Conditions to the Recent Improvement in Air Quality in China, Sci. Rep-UK., 6, 36404, doi: 10.1038/srep36404, 2016.

Yang, Y., H. Liao, and S. Lou: Increase in winter haze over eastern China in recent decades: Roles of variations in meteorological parameters and anthropogenic emissions, J. Geophys. Res. Atmos., 121, 13,050-013,065, doi: 10.1002/2016jd025136, 2016.

Zhang, H., S. Cheng, X. Wang, S. Yao, and F. Zhu: Continuous monitoring, compositions analysis and the implication of regional transport for submicron and fine aerosols in Beijing, China, Atmos. Environ., 195, 30-45, doi: 10.1016/j.atmosenv.2018.09.043, 2018.

Zhang, Y., J. Chen, H. Yang, R. Li, and Q. Yu: Seasonal variation and potential source regions of PM2.5-bound PAHs in the megacity Beijing, China: Impact of regional transport, Environ. Pollut., 231, 329-338, doi: 10.1016/j.envpol.2017.08.025, 2017.

Zhu, X., G. Tang, J. Guo, B. Hu, T. Song, L. Wang, J. Xin, W. Gao, C. Münkel, K. Schäfer, X. Li, and Y. Wang: Mixing layer height on the North China Plain and meteorological evidence of serious air pollution in southern Hebei, Atmos. Chem. Phys., 18, 4897-4910, doi: 10.5194/acp-18-4897-2018, 2018.

Zhu, X. W., G. Q. Tang, B. Hu, L. L. Wang, J. Y. Xin, J. K. Zhang, Z. R. Liu, C. Munkel, and Y. S. Wang: Regional pollution and its formation mechanism over North China Plain: A case study with ceilometer observations and model simulations, J. Geophys. Res-Atmos., 121, 14574-14588, doi: 10.1002/2016jd025730, 2016.